ACS OMEGA

Article

Cite This: ACS Omega 2019, 4, 19705−19709

http://pubs.acs.org/journal/acsodf

Alkyl Conformation and $\pi-\pi$ Interaction Dependent on Polymorphism in the 1,8-Naphthalimide (NI) Derivative

Kukhyun Jo,[†,⊥] Siwoo Lee,[†,⊥] Ahra Yi,[†] Tae-Yeol Jeon,[‡] Hyun Hwi Lee,*[,‡] Dohyun Moon,*[,‡] Dongmin M. Lee,[§] Jiyoung Bae,[§] Seung-Tae Hong,[§] Jinhwa Gene,[∥] Seung Geol Lee,*[,†] and Hyo Jung Kim*[,†]

[†]Department of Organic Material Science and Engineering, Pusan National University, Busan 46241, Republic of Korea

[‡]Pohang Accelerator Lab, POSTECH, Pohang, Gyeongbuk 37673, Republic of Korea

[§]Department of Energy Science and Engineering, DGIST (Daegu Gyeongbuk Institute of Science and Technology), Daegu 42988, Republic of Korea

[∥]Korean Research Institute of Standards and Science, Daejeon 34113, Republic of Korea

Supporting Information

ABSTRACT: The 1,8-naphthalimide (NI) derivative Lumogen F Violet 570 exhibits different photoluminescence (PL) and aggregation-caused quenching properties due to its crystal polymorphism, which depends on the solvent evaporation process in tetrahydrofuran solution. In the slow drying process, molecules aggregated into an energetically more stable form (time-dependent density functional theory calculation), of which the PL peak maximum was 453 nm, corresponding to blue emission at the 365 nm excitation. However, the fast evaporation process induces an energetically less stable form, with a PL peak maximum of 508 nm, corresponding to green emission. The main difference between the two crystal structures is the alkyl conformation, as confirmed by X-ray single-crystal analysis. Due to the different alkyl conformations, NI groups aggregated into more obliquely aligned structures that emit blue PL, which plays a role in weakening the $\pi-\pi$ interactions between molecules relative to green PL crystals. We found that the conformational stable molecular stacking induced instability in the electronic energy levels of the blue crystal compared to the green crystal.

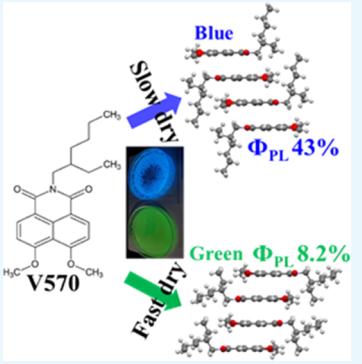

1. INTRODUCTION

1,8-Naphthalimide (NI) exhibits unique optical properties: it absorbs UV-region light and emits visible range light. It has been reported that the unique optical properties of NI are related to the transition of the electronic states of molecules from lowest unoccupied molecular orbital (LUMO) to highest occupied molecular orbital (HOMO) and vice versa.[1] It is easy to control the photophysical properties of NI because it is not difficult to chemically modify the naphtha group and N component of imide.[2,3] Therefore, NI has been widely used not only in the dye industry but also in various applications, including biomarker/biosensors,[4,5] organic light-emitting diodes,[6,7] solar cells,[8−15] luminescent solar concentrators,[16,17] and X-ray scintillators.[18]

Despite its unique optical properties and potential for diverse applications, NI has inevitable problems due to the enriched intermolecular π electrons of NI groups, which are related to strong intermolecular interactions induced by H-type aggregation, resulting in a reduction (quenching) of the photoluminescent (PL) efficiency.[19−21] To overcome H-type aggregation and aggregation-caused quenching (ACQ), researchers often adopt substituents in NI molecules to maintain the high fluorescence emission by interrupting the π interaction in the aggregate states of the molecules. Adopting a substituent is very effective for solving the ACQ problem, but it will unavoidably distort the physical/optoelectronic properties of the molecule by inducing chemical changes due to the substituent. Compared to a substituent, different intermolecular interactions could be expected in polymorphisms of a molecule. Organic molecules could have different molecular stackings, resulting in various crystal forms, without requiring any additional substituent. Despite their importance in the control of optoelectronic properties, polymorphisms have not been noted in NI molecules and few studies have been performed on them. In this work, we present two different crystalline states relating to the optoelectronic properties of the NI derivative Lumogen F Violet 570 (V570), which are dependent on the fabrication process in tetrahydrofuran (THF) solution. The ACQ could be suppressed in one crystal form, which emits blue PL due to the weakened π interaction in comparison to the other crystal form, which emits green PL.

Received: August 2, 2019
Accepted: October 22, 2019
Published: November 5, 2019

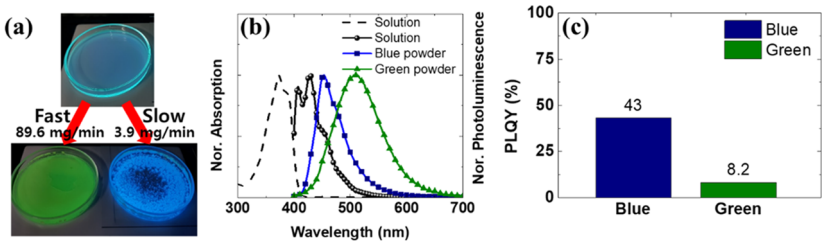

Figure 1. (a) Blue and green photoluminescence (PL) powders obtained by evaporating V570 solution under 365 nm irradiation. (b) Absorption (dash line) and emission (solid line) spectra of V570 solution and powders. (c) The photoluminescence quantum yields (PLQYs) of the blue and green powders.

Table 1. Crystal Data and Structure Refinement for V570 Blue and Green

identification code	blue		green	
crystal system	triclinic		triclinic	
space group	$P\bar{1}$		$P\bar{1}$	
unit cell dimensions	a = 8.0200(16) Å	α = 94.29(3)°	a = 7.2260(14) Å	α = 84.53(3)°
	b = 8.6280(17) Å	β = 103.15(3)°	b = 8.7570(18) Å	β = 81.88°
	c = 15.738(3) Å	γ = 115.59(3)°	c = 17.120(3) Å	γ = 66.39°
volume	937.7(4) Å^3		981.8(4) Å^3	
Z	2		2	
density (calculated)	1.308 mg/m^3		1.250 mg/m^3	
final R indices [$I > 2\sigma(I)$]	R_1 = 0.0536, wR_2 = 0.1481		R_1 = 0.0834, wR_2 = 0.2353	

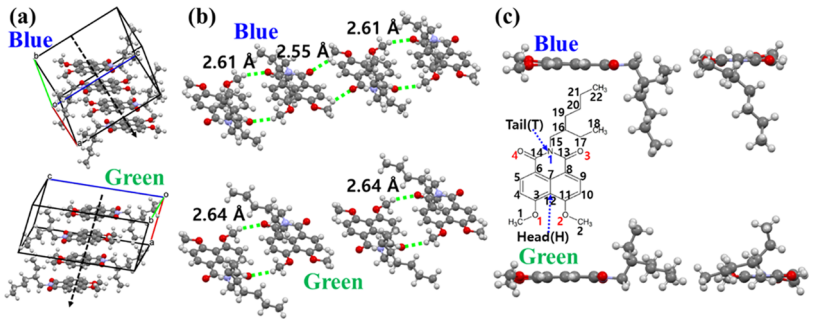

Figure 2. (a) Crystal structures repeating two unit cells along the a axis. (b) The hydrogen bonding formation in the blue and green forms. (c) The difference in alkyl group conformations in monomers between the blue and green forms.

2. RESULTS AND DISCUSSION

We dissolved 100 mg of V570 powder in 3 mL of tetrahydrofuran (THF) at room temperature and dried the solution at two evaporation rates, 3.9 (slow) and 89.6 mg/min (fast), as shown in Figure 1a. (The evaporation rate was measured by the evaporation weight of the solvent over time; see Figure S1 of the Supporting Information.) As shown in Figure 1a, the fast-dried powder was green under a 365 nm light-emitting lamp, while the slow-dried powder was blue. Figure 1b shows the absorbance and photoluminescence (PL) spectra of the solution (5.414×10^{-5} M, 0.002 wt %), blue and green powders. The absorption spectra of blue and green powders were measured using the diffuse reflection measurement method and Kubelka–Munk function, as shown in Figure S2.[22,23] In the case of the solution, the absorption peak was 372 nm and the PL maximum peak was 428 nm under the excitation condition of 365 nm. Under the same excitation conditions, the maximum PL emission peaks of the blue and green powders were at 453 and 508 nm, respectively. In both cases, the maximum PL wavelength was shifted to a longer wavelength in comparison to the solution. This was related to the larger intermolecular interactions in the powders than the solution. The photoluminescence quantum yield (PLQY) of the two powders was measured using a PL photometer with an integrating sphere, as shown in Figure S3, and it was calculated using a method proposed in the literature.[24] Compared to ~100% PLQY in low-doping film,[25] the PLQY was ~43% in the blue luminescent powder, while it was 8.3% in the green luminescent powder, as shown in Figure 1c. The suppressed PLQY in the two powders originated from the intermolecular π interactions in the solid, as previously mentioned.[26] We expected the π interactions to be weaker in the blue powder than in the green powder.

To understand the different PL properties, we carried out an X-ray single-crystal analysis of blue and green crystals at the 2D beamline in PLS-II (Pohang, Korea). The single crystals were obtained by slow evaporation of the THF solvent. Green crystals formed in the fast-drying state but could also be obtained by slow drying when small green seeds were prepared for the initial state. We tried to fabricate single crystals with acetone and obtained blue crystals at a low temperature (4 °C). The crystal structure of blue from acetone was consistent with the structure from THF, which was confirmed by single crystal X-ray crystallography and analysis. Compared with blue crystals, green crystals were not obtained in acetone.

DOI: 10.1021/acsomega.9b02377
ACS Omega 2019, 4, 19705−19709

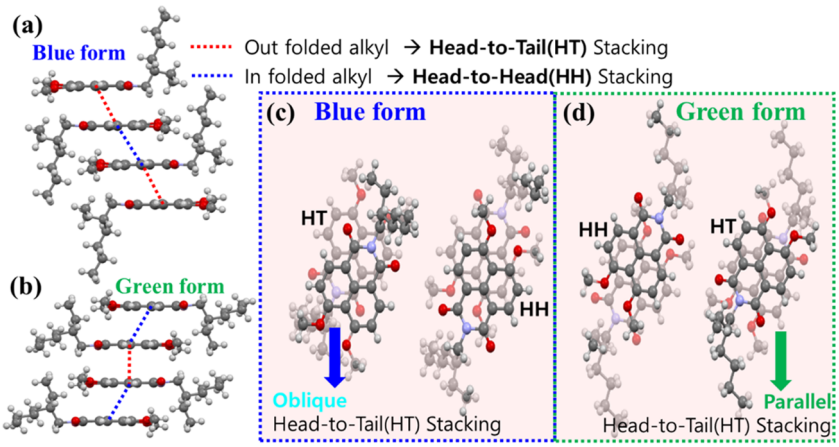

Figure 3. 1,8-Naphthalimide (NI) stacking structure in (a) the blue and (b) the green tetramer marked by connecting C7. The detailed stacking structures of intra- and interunit cells in (c) blue and (d) green NI planes (projection view).

In Table 1, we summarize the results of the crystal data from X-ray analysis (see Figure S4 for a detailed structure). In Figure S5, the powders and single crystals exhibited similar X-ray diffraction patterns and emission spectra. Hence, we can regard the crystal structures of the powders as the same as those of single crystals.

Based on the unit cell information, we compared the molecular stacking of the blue and green crystals, as shown in Figure 2.[27] The dotted arrow in Figure 2a is parallel to the *a* axis and is connected to C7 (Figure 3c) of a molecule in a unit cell. A unit cell consisted of two molecules, which were stacked in the *a*-direction, as shown in Figure 2a. In Figure 2b, the lengths of the hydrogen bonds between adjacent molecules were 2.61 and 2.55 Å. As a result, continuous hydrogen bonds formed in the blue crystals. On the other hand, green crystals did not form continuous hydrogen bonds between adjacent molecules due to the large bonding length (2.84 Å). The different stacking sequences between blue and green crystals were related to the different alkyl group conformations, as shown in Figure 2c. C15−C16 covalent bonding was in the opposite direction with respect to the NI planes of the blue and green crystals. Furthermore, the alkyl chains were more outstretched in the normal direction from the NI plane in the blue crystal than in the green crystal.

The NI plane stacking of the two-crystal form is depicted along the direction of the *a* axis, as shown in Figure 3. The NI stacking can be explained in terms of the positions of the neighboring NI planes and hindrance caused by alkyl conformation. Head-to-tail (HT) stacking refers to stacking between naphthalene (H) and imide (T) groups, while head-to-head (HH) stacking is vertical stacking between naphthalene (H) and naphthalene (H) groups. The NI stacking of blue crystal was HT and HH, in that order. Two alkyl chains were folded out from the NI stacking in the case of HT, and two alkyl chains were folded in towards the NI stacking in the case of HH. In the out-folding case, the NI groups could approach each other because there was relatively less interference with the neighboring alkyl chains due to the outstretched conformation. However, in the in-folding case, the NI group was more disturbed due to the in-folding conformation of the alkyl chains, and the NI group was spaced apart from the neighboring NI group.

Figure 3c,d shows top views of the HH and HT molecular stacking in blue and green crystals. Although the same HT stacking was observed in the blue and green crystals, the detailed structures of the HT were different. The two V570 molecules of the blue crystals had an oblique HT stacking, while the molecules of the green crystal had a parallel HT stacking. The difference in HT stacking can be explained by the length of the alkyl groups outside the NI plane, as mentioned previously (see Figure 2). Compared to the green crystal, the outstretched alkyl chain distance is long enough to interfere with the NI stacking in the blue crystal. Due to the lesser degree of overlap in the HT stacking, π bonding between two NI groups was weak in the blue crystal compared to the green crystal.

The total energy difference of blue and green crystals as a monomer state was calculated by using time-dependent density functional theory (TDDFT), as shown in Figure 4a. For

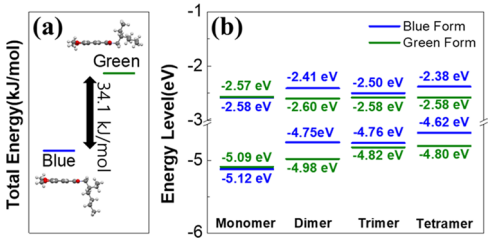

Figure 4. (a) Total energy diagram under the blue and green monomer conditions. (b) The highest occupied molecular orbital (HOMO) and lowest occupied molecular orbital (LUMO) state energy diagrams with increased V570 stacking along the *a* axis.

calculation, we used the double numerical basis sets with polarization level with the generalized gradient approximation of the Perdew−Burke−Ernzerhof functional.[28] We used all-electron Kohn−Sham wave functions and the spin-unrestricted DFT computation. The self-consistent field convergence of 10^{-6} Ha is obtained with a cut-off radius of 3.7 Å. The blue crystal has a more stable state than green crystal, and the energy difference between them was 34.1 kJ/mol. The blue crystal formed under slow evaporation, as mentioned previously, which implies that it was more stable than the green crystal. The results of our energy calculations are consistent with both the crystal formation conditions and our expectations. The NI group conformations of the blue and green crystals were similar. Therefore, we consider the energy

DOI: 10.1021/acsomega.9b02377
ACS Omega 2019, 4, 19705−19709

difference to be mainly related to the conformation of the alkyl group.

The energies of the HOMO and LUMO electronic states were calculated using the TDDFT method, as shown in Figure 4b. We calculated the electronic energy states from monomers to tetramers, for which the molecular stacking direction was along the *a* axis. The HOMO and LUMO energies of the blue and green crystals were almost the same in the monomer state because the HOMO and LUMO electronic states are derived not from the alkyl group but rather from the π electron-conjugated system of the NI group.[1] The optical band gap from the absorption spectrum (Figure S2) was 3.26 eV in the blue powder and 3.28 eV in the green powder.

In the dimer system, the molecular stacking corresponds to HT in the blue crystal, while it corresponds to HH in the green crystal. The HOMO and LUMO energies of blue are higher than those of green, which implies that HH is more stable than HT. In the case of the trimer system, HT and HH are included in the blue crystal, and HH and HT are included in the green crystal. As shown in Figure 3c,d, HHs of blue and green are similar, but HTs are oblique in the blue crystal. Therefore, the energy difference in the trimer system is mainly due to differences in HT states between the blue and green crystals. From our calculation, we confirmed that the oblique stacking was less stable than the parallel stacking because there were higher HOMO/LUMO energy states in the blue versus green crystals.

We also calculated the changes in the excitation energy through structural optimization in the first excited state (S_1), using TDDFT to elucidate the different emission characteristics of the blue and green crystals of V570. As shown in Figure S6, the excitation states obtained via optimization were not significantly different in the monomer states of the blue and green crystals. Therefore, we confirmed that the PL properties of blue and green were not derived from the monomer state but rather from the crystal structure.

3. CONCLUSIONS

We detected polymorphism in V570 molecules, i.e., blue and green emission crystals, depending on the evaporation rate of the solution during crystal formation. The PLQY of the green powder was as low as 8.2%, while it was 43% in the blue powder. We confirmed that the different PLQY properties and efficiencies originated from different π interactions, mainly relating to the alkyl chain conformation of the two states. The π interaction was weaker and HOMO/LUMO energy states were higher in the blue crystal in comparison to the green crystal. Interestingly, the conformational stable molecular stacking induced unstable electronic energy levels in the blue crystals compared to the green crystals.

■ ASSOCIATED CONTENT

Supporting Information

The Supporting Information is available free of charge at https://pubs.acs.org/doi/10.1021/acsomega.9b02377.

Detailed results data regarding the drying of the V570 solution: PLQY of powders; structure and PL of the powders and single crystals; lattice structure; and excited energy calculations were optimized in the initial excited state (PDF)

Blue single-crystal information (CIF)

Green single-crystal information (CIF)

■ AUTHOR INFORMATION

Corresponding Authors

*E-mail: hyojkim@pusan.ac.kr (H. J. Kim).
*E-mail: dmoon@postech.ac.kr (D. Moon).
*E-mail: hhleec@postech.ac.kr (H. H. Lee).
*E-mail: seunggeol.lee@pusan.ac.kr (S. G. Lee.).

ORCID

Tae-Yeol Jeon: 0000-0001-8786-4124
Dohyun Moon: 0000-0002-6903-0270
Seung-Tae Hong: 0000-0002-5768-121X
Seung Geol Lee: 0000-0001-7965-7387
Hyo Jung Kim: 0000-0002-9725-8598

Author Contributions

⊥These authors provided an equal contribution in the paper.

Notes

The authors declare no competing financial interest.

■ ACKNOWLEDGMENTS

This work was supported by the Basic Science Research Program through the National Research Foundation of Korea (NRF) funded by the Korean Government (NRF-2018R1A2B6005178, NRF-2015R1A5A1009962) and the Global collaborative R&D program (No. N0002095) of the Korea Institute for Advancement of Technology (KIAT) grant funded by the Korea Government Ministry of Trade, Industry and Energy (MOTIE), and the Korea Electric Power Corporation (CX72170050, R19XO01-11) and Samsung Electronics.

■ REFERENCES

(1) Jacquemin, D.; Perpète, E. A.; Scalmani, G.; Frisch, M. J.; Ciofini, I.; Adamo, C. Fluorescence of 1, 8-naphthalimide: a PCM-TD-DFT investigation. *Chem. Phys. Lett.* **2007**, *448*, 3−6.

(2) Duke, R. M.; Veale, E. B.; Pfeffer, F. M.; Kruger, P. E.; Gunnlaugsson, T. Colorimetric and fluorescent anion sensors: an overview of recent developments in the use of 1, 8-naphthalimide-based chemosensors. *Chem. Soc. Rev.* **2010**, *39*, 3936−3953.

(3) Banerjee, S.; Veale, E. B.; Phelan, C. M.; Murphy, S. A.; Tocci, G. M.; Gillespie, L. J.; Frimannsson, D. O.; Kelly, J. M.; Gunnlaugsson, T. Recent advances in the development of 1,8-naphthalimide based DNA targeting binders, anticancer and fluorescent cellular imaging agents. *Chem. Soc. Rev.* **2013**, *42*, 1601−1618.

(4) Jia, T.; Fu, C.; Huang, C.; Yang, H.; Jia, N. Highly sensitive naphthalimide-based fluorescence polarization probe for detecting cancer cells. *ACS Appl. Mater. Interfaces* **2015**, *7*, 10013−10021.

(5) Gao, Y. G.; Tang, Q.; Shi, Y. D.; Zhang, Y.; Lu, Z. L. 1,8-Naphthalimide modified [12]aneN3 compounds as selective and sensitive probes for Cu^{2+} ions and ATP in aqueous solution and living cells. *Talanta* **2016**, *152*, 438−446.

(6) Kolosov, D.; Adamovich, V.; Djurovich, P.; Thompson, M. E.; Adachi, C. 1, 8-naphthalimides in phosphorescent organic LEDs: the interplay between dopant, exciplex, and host emission. *J. Am. Chem. Soc.* **2002**, *124*, 9945−9954.

(7) Ulla, H.; Garudachari, B.; Satyanarayan, M. N.; Umesh, G.; Isloor, A. M. Blue organic light emitting materials: Synthesis and characterization of novel 1,8-naphthalimide derivatives. *Opt. Mater.* **2014**, *36*, 704−711.

(8) Alonso-Álvarez, D.; Ross, D.; Richards, B. S. In *Luminescent Down-Shifting for CdTe Solar Cells: A Review of Dyes and Simulation of Performance*, 38th IEEE Photovoltaic Specialists Conference; IEEE, 2012; pp 000009−000014.

(9) Danos, L.; Parel, T.; Markvart, T.; Barrioz, V.; Brooks, W. S. M.; Irvine, S. J. C. Increased efficiencies on CdTe solar cells via

DOI: 10.1021/acsomega.9b02377
ACS Omega 2019, 4, 19705−19709

luminescence down-shifting with excitation energy transfer between dyes. *Sol. Energy Mater. Sol. Cells* **2012**, *98*, 486−490.
(10) Ross, D.; Klampaftis, E.; Fritsche, J.; Bauer, M.; Richards, B. S. Increased short-circuit current density of production line CdTe mini-module through luminescent down-shifting. *Sol. Energy Mater. Sol. Cells* **2012**, *103*, 11−16.
(11) Ross, D.; Alonso-Alvarez, D.; Klampaftis, E.; Fritsche, J.; Bauer, M.; Debije, M. G.; Fifield, R. M.; Richards, B. S. The impact of luminescent down shifting on the performance of CdTe photovoltaics: impact of the module vintage. *IEEE J. Photovoltaics* **2014**, *4*, 457−464.
(12) Bella, F.; Griffini, G.; Gerosa, M.; Turri, S.; Bongiovanni, R. Performance and stability improvements for dye-sensitized solar cells in the presence of luminescent coatings. *J. Power Sources* **2015**, *283*, 195−203.
(13) Alonso-Álvarez, D.; Ross, D.; Klampaftis, E.; McIntosh, K. R.; Jia, S.; Storiz, P.; Stolz, T.; Richards, B. S. Luminescent down-shifting experiment and modelling with multiple photovoltaic technologies. *Prog. Photovoltaics* **2015**, *23*, 479−497.
(14) Solodovnyk, A.; Kick, C.; Osvet, A.; Egelhaaf, H. J.; Stern, E.; Batentschuk, M.; Forberich, K.; Brabec, C. J. Optimization of Solution-Processed Luminescent Down-Shifting Layers for Photovoltaics by Customizing Organic Dye Based Thick Films. *Energy Technol.* **2016**, *4*, 385−392.
(15) Solodovnyk, A.; Kick, C.; Osvet, A.; Egelhaaf, H. J.; Stern, E.; Batentschuk, M.; Forberich, K.; Brabec, C. J. Computational optimization and solution-processing of thick and efficient luminescent down-shifting layers for photovoltaics. *Proc. SPIE* **2016**, *9743*, No. 97430G.
(16) van Sark, W. G. J. H. M.; Barnham, K. W. J.; Slooff, L. H.; Chatten, A. J.; Büchtemann, A.; Meyer, A.; McCormack, S. J.; Koole, R.; Farrell, D. J.; Bose, R.; Bende, E. E.; Burgers, A. R.; Budel, T.; Quilitz, J.; Kennedy, M.; Meyer, T.; Donega, C. D. M.; Meijerink, A.; Vanmaekelbergh, D. Luminescent Solar Concentrators-A review of recent results. *Opt. Express* **2008**, *16*, 21773−21792.
(17) McKenna, B.; Evans, R. C. Towards efficient spectral converters through materials design for luminescent solar devices. *Adv. Mater.* **2017**, *29*, No. 1606491.
(18) Dalla Palma, M.; Carturan, S. M.; Degerlier, M.; Marchi, T.; Cinausero, M.; Gramegna, F.; Quaranta, A. Non-toxic liquid scintillators with high light output based on phenyl-substituted siloxanes. *Opt. Mater.* **2015**, *42*, 111−117.
(19) Gopikrishna, P.; Meher, N.; Iyer, P. K. Functional 1, 8-naphthalimide AIE/AIEEgens: recent advances and prospects. *ACS Appl. Mater. Interfaces* **2018**, *10*, 12081−12111.
(20) Yuan, H.; Wang, K.; Yang, K.; Liu, B.; Zou, B. Luminescence properties of compressed tetraphenylethene: the role of intermolecular interactions. *J. Phys. Chem. Lett.* **2014**, *5*, 2968−2973.
(21) Feng, F.; Yang, J.; Xie, D.; McCarley, T. D.; Schanze, K. S. Remarkable photophysics and amplified quenching of conjugated polyelectrolyte oligomers. *J. Phys. Chem. Lett.* **2013**, *4*, 1410−1414.
(22) Kubelka, P.; Franz, M. An article on optics of paint layers. *Z. Tech. Phys.* **1931**, *12*, 593−601.
(23) Džimbeg-Malčić, V.; Barbarić-Mikočević, Ž.; Itrić, K. Kubelka-Munk theory in describing optical properties of paper (I). *Teh. Vjesn.* **2011**, *18*, 117−124.
(24) de Mello, J. C.; Wittmann, H. F.; Friend, R. H. An improved experimental determination of external photoluminescence quantum efficiency. *Adv. Mater.* **1997**, *9*, 230−232.
(25) Wilson, L. R.; Richards, B. S. Measurement method for photoluminescent quantum yields of fluorescent organic dyes in polymethyl methacrylate for luminescent solar concentrators. *Appl. Opt.* **2009**, *48*, 212−220.
(26) Katoh, R.; Suzuki, K.; Furube, A.; Kotani, M.; Tokumaru, K. Fluorescence quantum yield of aromatic hydrocarbon crystals. *J. Phys. Chem. C* **2009**, *113*, 2961−2965.
(27) Macrae, C. F.; Bruno, I. J.; Chisholm, J. A.; Edgington, P. R.; McCabe, P.; Pidcock, E.; Rodriquez-Monge, L.; Taylor, R.; Streek, J. V. D.; Wood, P. A. Mercury CSD 2.0—new features for the visualization and investigation of crystal structures. *J. Appl. Crystallogr.* **2008**, *41*, 466−470.
(28) Perdew, J. P.; Burke, K.; Wang, Y. Generalized gradient approximation for the exchange-correlation hole of a many-electron system. *Phys. Rev. B* **1996**, *54*, 16533.

DOI: 10.1021/acsomega.9b02377
ACS Omega 2019, 4, 19705−19709